

# Lawrence Berkeley National Laboratory

## LBL Publications

### Title

Optimizing Perovskite Thin-Film Parameter Spaces with Machine Learning-Guided Robotic Platform for High-Performance Perovskite Solar Cells

### Permalink

<https://escholarship.org/uc/item/5gb2s637>

### Journal

Advanced Energy Materials, 13(48)

### ISSN

1614-6832

### Authors

Zhang, Jiyun

Liu, Bowen

Liu, Ziyi

et al.

### Publication Date

2023-12-01

### DOI

10.1002/aenm.202302594

### Copyright Information

This work is made available under the terms of a Creative Commons Attribution License, available at <https://creativecommons.org/licenses/by/4.0/>

Peer reviewed

# Optimizing Perovskite Thin-Film Parameter Spaces with Machine Learning-Guided Robotic Platform for High-Performance Perovskite Solar Cells

Jiyun Zhang,\* Bowen Liu, Ziyi Liu, Jianchang Wu, Simon Arnold, Hongyang Shi, Tobias Osterrieder, Jens A. Hauch, Zhenni Wu, Junsheng Luo, Jerrit Wagner, Christian G. Berger, Tobias Stubhan, Frederik Schmitt, Kaicheng Zhang, Mykhailo Sytnyk, Thomas Heumueller, Carolin M. Sutter-Fella, Ian Marius Peters, Yicheng Zhao,\* and Christoph J. Brabec\*

Simultaneously optimizing the processing parameters of functional thin films remains a challenge. The design and utilization of a fully automated platform called SPINBOT is presented for the engineering of solution-processed functional thin films. The SPINBOT is capable of performing experiments with high sampling variability through the unsupervised processing of hundreds of substrates with exceptional experimental control. Through the iterative optimization process enabled by the Bayesian optimization (BO) algorithm, the SPINBOT explores an intricate parameter space, continuously improving the quality and reproducibility of the produced thin films. This machine learning (ML)-guided reliable SPINBOT platform enables the acceleration of the optimization process of perovskite solar cells via a simple photoluminescence characterization of films. As a result, this study arrives at an optimal film that, when processed into a solar cell in an ambient atmosphere, immediately yields a champion power conversion efficiency (PCE) of 21.6% with satisfactory performance reproducibility. The unsealed devices retain 90% of their initial efficiency after 1100 h of continuous operation at 60–65 °C under metal-halide lamps. It is anticipated that the integration of robotic platforms with the intelligent algorithm will facilitate the widespread adoption of effective autonomous experimentation to address the evolving needs and constraints within the materials science research community.

## 1. Introduction

Solution-processed thin films commonly used in organic,<sup>[1–3]</sup> dye-sensitized,<sup>[4,5]</sup> and perovskite solar cells (PSCs)<sup>[6–8]</sup> are an attractive alternative to crystalline wafers due to easier fabrication processes, lower manufacturing cost, and potentially higher power-per-weight of the materials.<sup>[9]</sup> Developing a reliable manufacturing technique for solution-processed thin films requires process optimization in a highly dimensional parameter space. Simultaneously optimizing the processing parameters of thin films is time-consuming and labor-intensive because of the large number of closely correlated parameters.<sup>[10]</sup> This non-orthogonality of the parameter space has a profound influence on identifying unique causal relations between processing conditions and the microstructure and properties of the final semiconducting layers.<sup>[11]</sup>

J. Zhang, J. Wu, S. Arnold, T. Osterrieder, J. A. Hauch, Z. Wu, J. Wagner, C. G. Berger, F. Schmitt, M. Sytnyk, T. Heumueller, I. M. Peters, C. J. Brabec  
Helmholtz-Institute Erlangen-Nürnberg (HI ERN)  
Department of High Throughput Methods in Photovoltaics  
Helmholtz-Institute Erlangen-Nürnberg (HI ERN)  
91058 Erlangen, Germany  
E-mail: jiyun.zhang@fau.de; christoph.brabec@fau.de

The ORCID identification number(s) for the author(s) of this article can be found under <https://doi.org/10.1002/aenm.202302594>

© 2023 The Authors. Advanced Energy Materials published by Wiley-VCH GmbH. This is an open access article under the terms of the Creative Commons Attribution License, which permits use, distribution and reproduction in any medium, provided the original work is properly cited.

DOI: 10.1002/aenm.202302594

J. Zhang, B. Liu, J. Wu, S. Arnold, H. Shi, J. A. Hauch, Z. Wu, K. Zhang, T. Heumueller, C. J. Brabec  
Faculty of Engineering  
Department of Material Science  
Materials for Electronics and Energy Technology (i-MEET)  
Friedrich-Alexander-University Erlangen-Nuremberg (FAU)  
91058 Erlangen, Germany  
B. Liu, Z. Liu, J. Luo, Y. Zhao  
State Key Laboratory of Electronic Thin Films and Integrated Devices  
School of Electronic Science and Engineering  
University of Electronic Science and Technology of China (UESTC)  
Chengdu 611731, P. R. China  
E-mail: zhaoyicheng@uestc.edu.cn

At the same time, knowledge-based materials science is a domain where manual routines and traditional trial-and-error approaches are still predominant. One typical example is the optimization of functional thin film processing for device operation. Identifying processing conditions for high-performance devices, in particular, still relies heavily on the empirical decisions of human experts in single laboratories and underlies the restrictions of ad-hoc trials and non-holistic approaches. As a result, these “optimized” procedures typically work for a single lab but otherwise suffer from poor intra-lab reproducibility and inter-lab transferability. Particularly in the field of perovskites, this is reflected by the huge number of published processing conditions and significant standard deviation in device performance.<sup>[12–14]</sup>

Automated research platforms, commonly known as Materials Acceleration Platforms (MAPs), have been introduced to explore the realms in the multi-dimensional parameter space. These MAPs have already achieved significant successes in addressing high-dimensional problems in fields such as experimental life sciences, chemistry, and physics, with great precision, speed, and accuracy.<sup>[15–18]</sup> The scientific community has recognized the potential of MAPs to revolutionize materials research and development processes in several ways such as accelerated discovery, efficiency and cost savings, improved material performance, enhanced collaboration, and feasible knowledge sharing.<sup>[19–21]</sup> Noteworthy examples include the research work by MacLeod et al., who introduced a modular robotic platform called Ada driven by a model-based optimization algorithm to optimize organic and palladium films by modifying their composition and processing conditions.<sup>[22,23]</sup> Similarly, Zhao et al. reported a robotic platform framework that integrates data mining, controllable synthesis, and inverse design for achieving targeted colloidal nanocrystal morphologies.<sup>[24]</sup> In our previous work, we employed a robotic platform, Tecan, to synthesize and screen hundreds of multi-cation perovskite compositions for perovskite devices with long-term operational stability.<sup>[25,26]</sup> Additionally, by coupling the Gaussian Process Regression (GPR) prediction approach based on optical absorption features,<sup>[27]</sup> we autonomously explored over 100 process conditions to optimize the efficiency performance and photo-stability of organic photovoltaics (OPVs).<sup>[28]</sup> The methodology of integrating automation in energy thin film materials research, especially for perovskite materials, is drawing ever-increasing attention.<sup>[6,29–31]</sup>

To effectively leverage MAPs, sequential Machine Learning (ML)-driving tools, such as the Bayesian Optimization (BO) method, have been widely adopted as robust optimization strategies for material exploration.<sup>[22,32,33]</sup> The BO method, often employing the GPR model, has proven to be efficient in optimizing problems with multi-dimensional variable spaces by providing a visualized mapping between input and target properties.<sup>[34,35]</sup> Combining MAPs with ML-driving algorithms for the fabrication and characterization of solution-processed PV thin film materi-

als will undoubtedly contribute to the acceleration of materials discovery by making high-dimensional parameter optimization more manageable.<sup>[19,28,36,37]</sup>

In this report, we introduce a fully automated spin-coating platform called “SPINBOT” (Figure 1A) for the engineering of solution-processed functional thin film materials. Through integrating a BO algorithm, the SPINBOT effectively optimized the manufacturing parameters of perovskite thin films in a complex, multi-dimensional parameter space. As a result, this ML-guided reliable platform enables us to accelerate the optimization process of perovskite solar cells via a simple PL characterization of films and make a perovskite device with a champion efficiency of 21.6%. Moreover, unsealed devices from the same batch exhibited satisfactory performance reproducibility and photo-thermal stability, retaining 90% ± 3% of their initial efficiency after 1100 h of continuous aging at 60–65 °C in Nitrogen atmosphere under metal-halide lamps.

## 2. Results and Discussion

### 2.1. The Automated SPINBOT Platform and Workflow

Figure 1A and Figure S1 (Supporting Information) show the picture and schematic diagram of the SPINBOT platform. The robot component utilized for movement along four axes (X-, Y-, Z- and R-axis) is a Selective Compliance Assembly Robot Arm (SCARA) with high speed, flexibility, and rigidity (Figure S2, Supporting Information). SCARA performs multiple selective tasks repetitively with the high accuracy, efficiency, and precision required for high-throughput device processing. A liquid handling pipetting (LHP) module and a customized substrate-handling gripper (Figure S3, Supporting Information) are mounted to the robot arm. The LHP module driven by a pressure-based liquid-level sensing mode (Figure S4, Supporting Information) is used to aspirate, dispense, and mix liquid solutions. The substrate gripper moves the substrates into and out of the system. Thin films are produced with a customized mini-spin coater in a quasi-static on-the-fly spin coating mode (Figure S5, Supporting Information).<sup>[38]</sup> A typical deposition process with this tool looks like this: the precursor is dispensed on a slowly rotating substrate while the pipette tip slowly moves from the central site to the periphery of the substrate. The spin coater then accelerates to its target velocity after the solution is completely dispensed. The LHP with a newly mounted tip aspirates and then dispenses the anti-solvent onto a substrate with a certain tip height and dispensing speed at the scheduled timing. The carrier containing eight film-coated substrates is then transferred to the hotplates by the gripper for two-step thermal annealing (Figure S6, Supporting Information). An in-house characterization platform is used to carry out optical measurements, including recording the UV–vis absorption spectrum, the steady-state photoluminescence (PL) spectrum, and the time-resolved photoluminescence (TRPL) spectrum (Figure 1B; Figure S7, Supporting Information).<sup>[26,39–44]</sup> Multiple positions with a regular pattern on the front and back sides of samples were characterized to evaluate film reproducibility, homogeneity, and quality. The entire streamlined fabrication process and measurement of thin films can be found in the Video S1 (Supporting Information).

S. Arnold, C. M. Sutter-Fella  
Molecular Foundry  
Lawrence Berkeley National Laboratory  
Berkeley, CA 94720, USA

T. Stubhan  
SCIPRIOS GmbH  
90429 Nuremberg, Germany

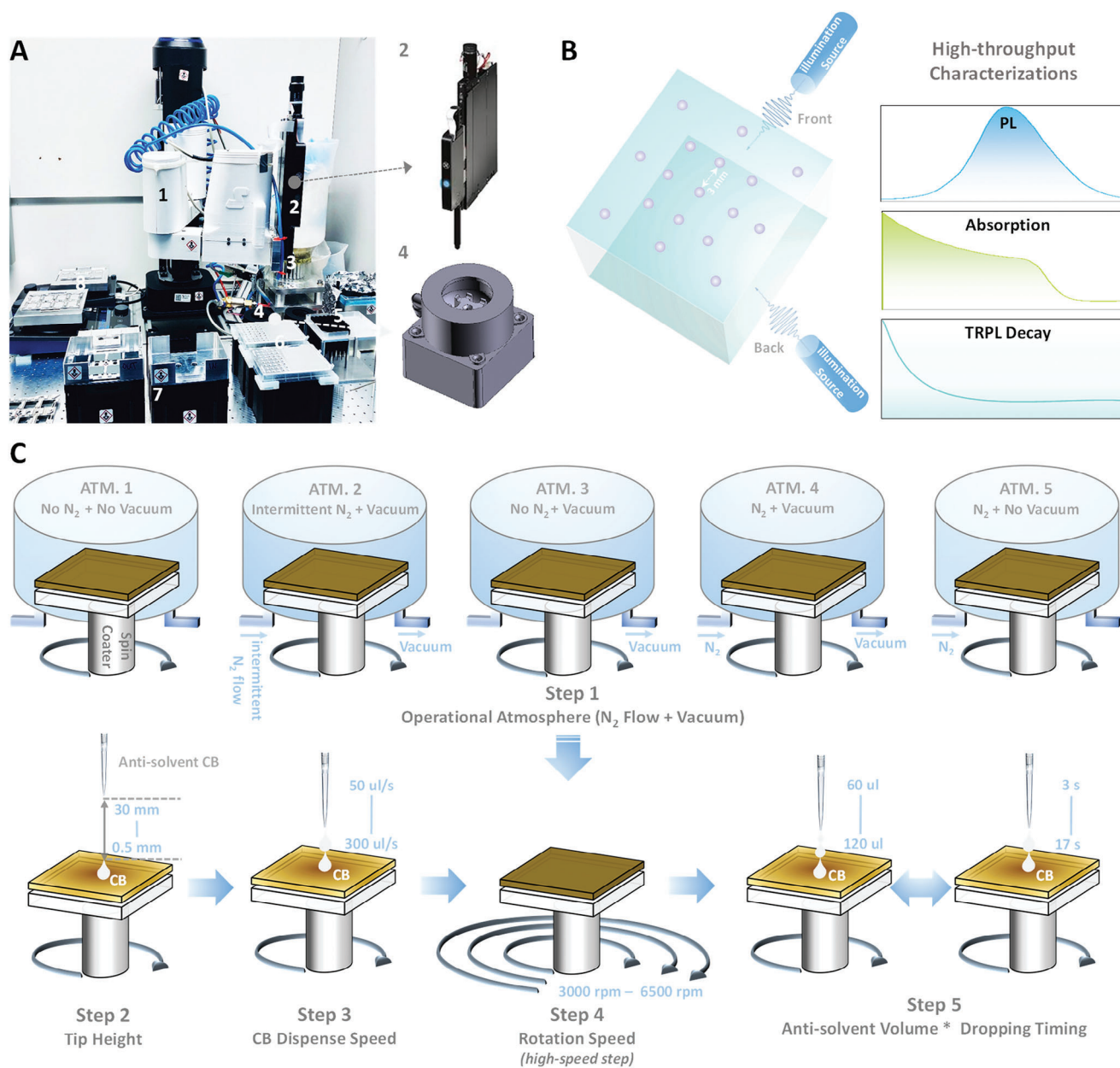


**Figure 1.** The SPINBOT platform and the step-by-step optimization workflow. A) Photograph of the SPINBOT platform. Part 1. robot arm with four movement axes: X-, Y-, Z- and R-axis; 2. liquid handling pipette; 3. substrate handling gripper; 4. mini spin coaters; 5. pipette tips; 6. 96-well microplates as solution-vessel for solutions stocking and anti-solvents; 7. carrier holders; 8. hotplates. B) Schematic of the high-throughput (HT) characterization for samples fabricated via the SPINBOT platform. Characterization methods include steady-state PL, UV-vis absorption, and time-resolved PL spectra. C) Schematic of the step-by-step optimization workflow. The sequencing optimization process consists of five steps, with a total of 61 experimental parameter combinations. Step 1: operational atmospheres (ATM.) inside the spin-coater chamber; Step 2: tip height during CB quenching; Step 3: dispense velocity of CB; Step 4: rotation speed during high-speed stage; Step 5: combination of CB volume and feeding timing.

## 2.2. Step-By-Step Optimization Method for Perovskite Thin Films

The ability to produce high-quality, well-organized datasets while also controlling typically uncontrolled parameters (e.g., the time between process steps, tip height, and ejection speed of spin-coating dispense nozzle) adds a new dimension of optimization parameters to the SPINBOT platform. The design of the experiments covered a multi-parameter space consisting of 5 optimiza-

tion steps, with a total of 61 parameter combinations (Tables S1 and S2, Supporting Information). The homogeneity and quality of the perovskite thin films were optimized by elaborately designing film fabrication processing at different atmospheres and different anti-solvent quenching parameters with various tip heights, rotation speeds, anti-solvent dropping volume, and dispense timings (steps 1 to 5, Figure 1c). PL measurements were taken as proxies for device performance. Rather than processing

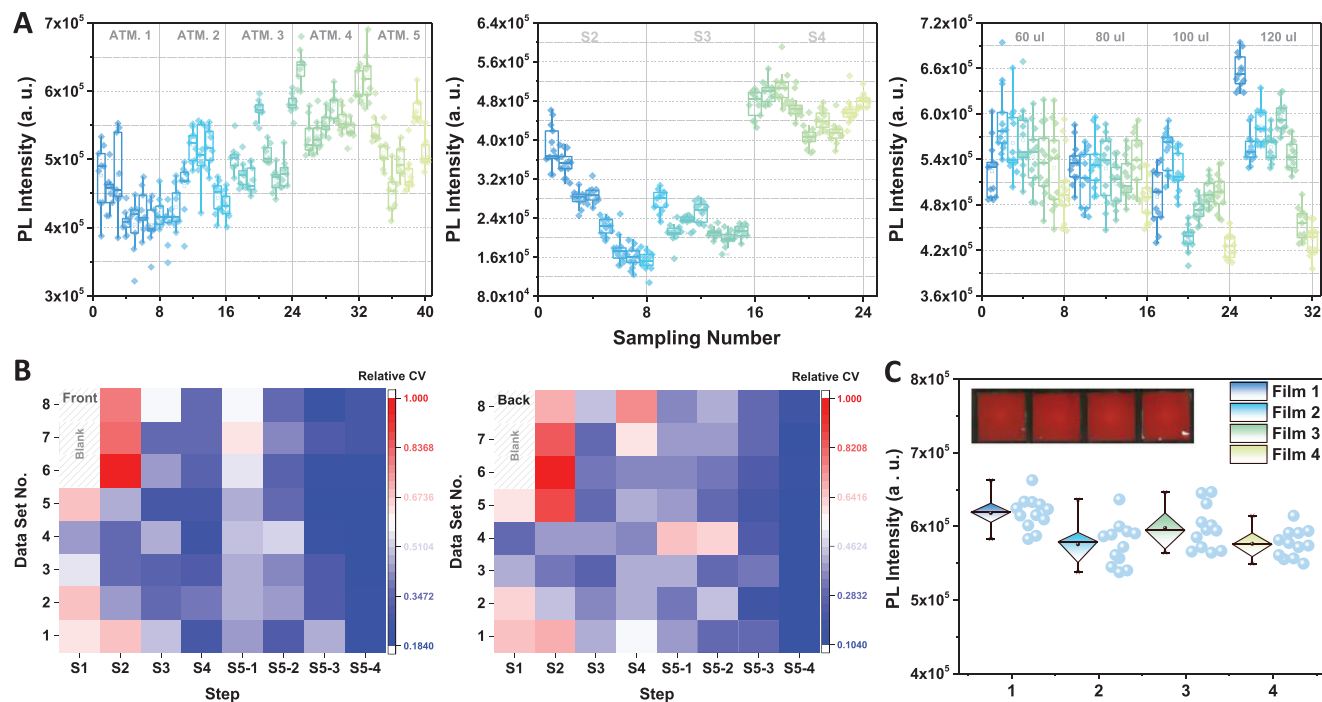


**Figure 2.** Results of step-by-step process optimization of the film homogeneity and reproducibility performed by the automated SPINBOT platform. A) Grouped box plots depicting the PL intensity of thin films produced in different steps. B) Color maps of the relative coefficient variation for the front (film) side and back (glass) side of the samples, respectively. C) Box plot of the PL intensity for the films produced under the found optimum conditions. The inserted photograph with LED backlight panel shows the four perovskite films produced under the found optimum conditions.

whole devices, the SPINBOT optimized film homogeneity and quality of organic–inorganic halide perovskites according to criteria such as PL peak position, intensity, and spatial homogeneity of the PL emission.

To evaluate the effect of experimental parameters on the sample properties, we first converged the absorption spectra from all test points of each sample. The films show negligible absorption difference, even the initial thin films produced under different atmospheres, indicating sufficient thickness reproducibility (Figure S8, Supporting Information). The time-resolved PL spectra show similar results (Figure S9, Supporting Information). We then chose the PL spectrum, a more sensitive indicator of film homogeneity and quality, as our main target for evaluating fabrication reproducibility under various parameters.<sup>[45,46]</sup>

**Figure 2** shows the results of sequential optimization for thin film reproducibility and quality. As shown in Figure 2A, the different operational atmosphere (ATM.) within the spin-coater chamber, tip height, combinatorial mode of CB dispense volume, and timing are identified as the dominant parameters influencing the final PL intensity. Compared with films fabricated in an ambient atmosphere (ATM. 1 and 2), the films with improved uniformity and quality can be achieved through the application of an  $N_2$  gas flow or/and vacuum operation due to the creation of a better-controlled atmosphere and rapid removal of residual solvent (Table S3, Supporting Information).<sup>[47,48]</sup> The effect of tip height is rarely reported in the literature owing to the impossibility of controlling the tip height within 0.1 mm error with manual operation. Our robotic platform provides the feasibility to achieve this accuracy and allows us to identify a further critical

parameter in perovskite processing. The SPINBOT reported an almost linear decline of PL intensity with increasing tip height, in which the intensity decreased threefold from the lowest distance to the highest distance. The statistical distribution of the PL peak position and grouped box plots of the integrated PL intensity for the films were also extracted and analyzed (Figures S10 and S11, Supporting Information). Figure S9 (Supporting Information) shows that the PL peak position variance is gradually minimized (from 6.14 to 0.51 nm) through step-by-step optimization. A similar trend is also unveiled by the analytical results of FWHM and peak positions extracted from the substrate backside (Figure S12, Supporting Information). To have a direct observation and quantitative evaluation of the PL intensity variance, the contour value maps were plotted to reveal the PL intensity distribution as a function of 13 specific characterization positions in the films. As shown in Figure S13 (Supporting Information), the films with the best homogeneity were obtained with 2–3 mm tip heights (step 2), which means a trade-off between the benefits of PL intensity and homogeneity. As the dropping volume of the anti-solvent was increased, the peak position of the films decreased. At the same time, the PL intensity remained stable until the volume increased to 120  $\mu\text{L}$ , which led to a gradual decrease with the prolongation of CB feeding time (Figure S14, Supporting Information). The film with the highest photoluminescence intensity and excellent homogeneity is finally achieved when the CB dispense volume is 120  $\mu\text{L}$  at 3 s (CB quenching timing).

To better visualize the variability evolution of samples produced over the parameter space as the optimization progresses,

we further summarized the color maps of relative coefficient variation for the front and back sides of each film (Figure 2B).<sup>[49,50]</sup> The color maps explicitly manifest the correlations between different parameter combinations and their impact on film homogeneity. The optimum parameter found in each step through this analytical approach is consistent with the previous results. As a result, the films with high reproducibility and quality (lowest CV: 0.184 and 0.104 for the front and back sides, respectively) were finally achieved after step-by-step optimization performed by the automated SPINBOT platform. To confirm the exceptional process control and reproducibility of the automated platform for film processing under the found optimum conditions, we repeated producing several thin films with the same processing parameter. As a result, a narrow coefficient variance of 0.74% in photoluminescence intensity for the processed films was achieved (Figure 2C), demonstrating that complex solution processing can be highly reproducible to produce high-quality thin films with such a reliable SPINBOT platform in the lab. Considering the drawbacks of the traditional step-by-step optimization method such as limited parameter ranges and local optimal, high-dimensional optimization tasks may not be adequately addressed even with sophisticated design of experiments (DoE). Machine learning (ML)-driven systems could offer a valuable framework for effectively exploring and expanding the range of parameter sets within the vast and limitless space of materials research. Therefore, in our subsequent study, we chose a Bayesian Optimization (BO)-guided iterative optimization strategy to further explore the global optimization of parameters.

### 2.3. BO-Guided Closed-Loop Optimization Method for Perovskite Thin Films

Figure 3A illustrates the experimental workflow of the BO-guided closed-loop optimization approach. This autonomous workflow involves iterative experimentation with the objective of discovering the optimal manufacturing parameters for perovskite thin films with high-quality (highest PL intensity) and high homogeneity (lowest PL peak CV and intensity CV) compared to the optimal results obtained previously. The initial set of parameters for the first round is randomly selected from the unlimited parameters library using the BO algorithm. The thin films, fabricated through the SPINBOT, are subsequently characterized using an in-house HT-spectrometer. The resulting data is analyzed by the BO algorithm framework, recommending two or three parameter sets for the subsequent iteration round. After multiple rounds of optimization, the optimal parameter set is finally determined and translated into perovskite device fabrication.

In total, we conducted eight sequential rounds of prediction and validation with only three new experiments for each target. The evaluation of experimental values, including peak CV, average intensity, and intensity CV, extracted from the PL spectra, along with the corresponding predicted values and error ranges, are presented in Figure 3B–D. Initially, the thin films fabricated under randomly selected parameter sets (Round 0) exhibit poor performance, indicated by high CV values and low PL intensity. The quality and reproducibility of the samples were gradually improved when the BO algorithm-recommended sets were adopted.

As shown in Figure 3B, the average PL intensity values exhibited considerable fluctuations during the initial three rounds, followed by a gradual increase until reaching a peak intensity in the final two rounds. The average PL intensity achieved through this approach was significantly higher than the previous sequential process method. After 3–4 rounds, the experimental CV values of PL intensity (Figure 3C) align well with the value interval predicted by the algorithm, with a final CV value of  $\approx 0.04$ , significantly lower than the lowest value obtained using the step-by-step optimization method. Despite slight fluctuations, the evolution of PL peak CV values demonstrates a consistent decreasing trend compared to the Round 0 samples, ultimately reaching an optimal value in the final round (Figure 3D). These favorable outcomes demonstrate that through the iterative optimization process facilitated by the BO algorithm, the SPINBOT systematically explores a complex parameter space, continuously improving the quality and performance of the produced thin films. As a result, the optimal solution (a higher-speed step at 4660 rpm for 22 s, 150  $\mu\text{L}$  CB was dropped onto the film with a dispense height of 2.6 mm and velocity of  $165 \mu\text{L s}^{-1}$  at 6 s, followed by annealing at 100 °C for 10 min and 150 °C for 5 min in the air) has been identified. This particular parameter set demonstrates promising potential for the fabrication of high-performance perovskite solar cells.

Figure 3E illustrates the operational optimization principle of the customized BO-guided iterative method and step-by-step approach. The step-by-step method identifies an optimal parameter set within a limit parameter library and narrows it down to a set of optimal candidates through a sequential process. By analyzing and leveraging the optimal parameter set at each round, the ML-guided closed-loop optimization workflow facilitates efficient and effective experimentation. This approach avoids producing and evaluating thin films with poorly estimated coefficient variations and allocates more resources toward the highly reproducible portion of the parameter space. As a result, the ML-guided optimization method not only overcomes the limitations of the step-by-step optimization process but also leads to a substantial enhancement in the quality of the thin films through a global optimization strategy.

### 2.4. Device Characterizations and Stability Performance

To understand the relevance of the PL proxy based film optimization on device performance, perovskite solar cells (PSCs) with an n–i–p structure of ITO/  $\text{SnO}_2$ -PEIE (polyethylenimine)/ perovskite/ PDCBT (poly[2,2'′-bis[(2-butyloctyl)oxy] carbonyl [2,2′5′,2′′:5′′,2′′′-quaterthiophene]–5,5′′′-diyl])/ PTAA-BCF ((tris (pentafluorophenyl) borane-doped poly(triarylamine))/ Au (see detailed device architecture in Figure 4A) were fabricated. Here the perovskite absorbers were coated by the SPINBOT with the optimal parameter sets for film processing in ambient air. All other layers of the devices were then deposited manually in an  $\text{N}_2$ -filled glovebox. Representative current density versus voltage ( $J$ – $V$ ) curves and performance statistics measured under Air Mass 1.5 Global (AM 1.5 G) solar irradiation ( $100 \text{ mW cm}^{-2}$ ) are shown in Figure 4B and Figure S15 (Supporting Information) for the PSCs with various film processing. From the extracted device performances (Figure S16, Supporting Information), the

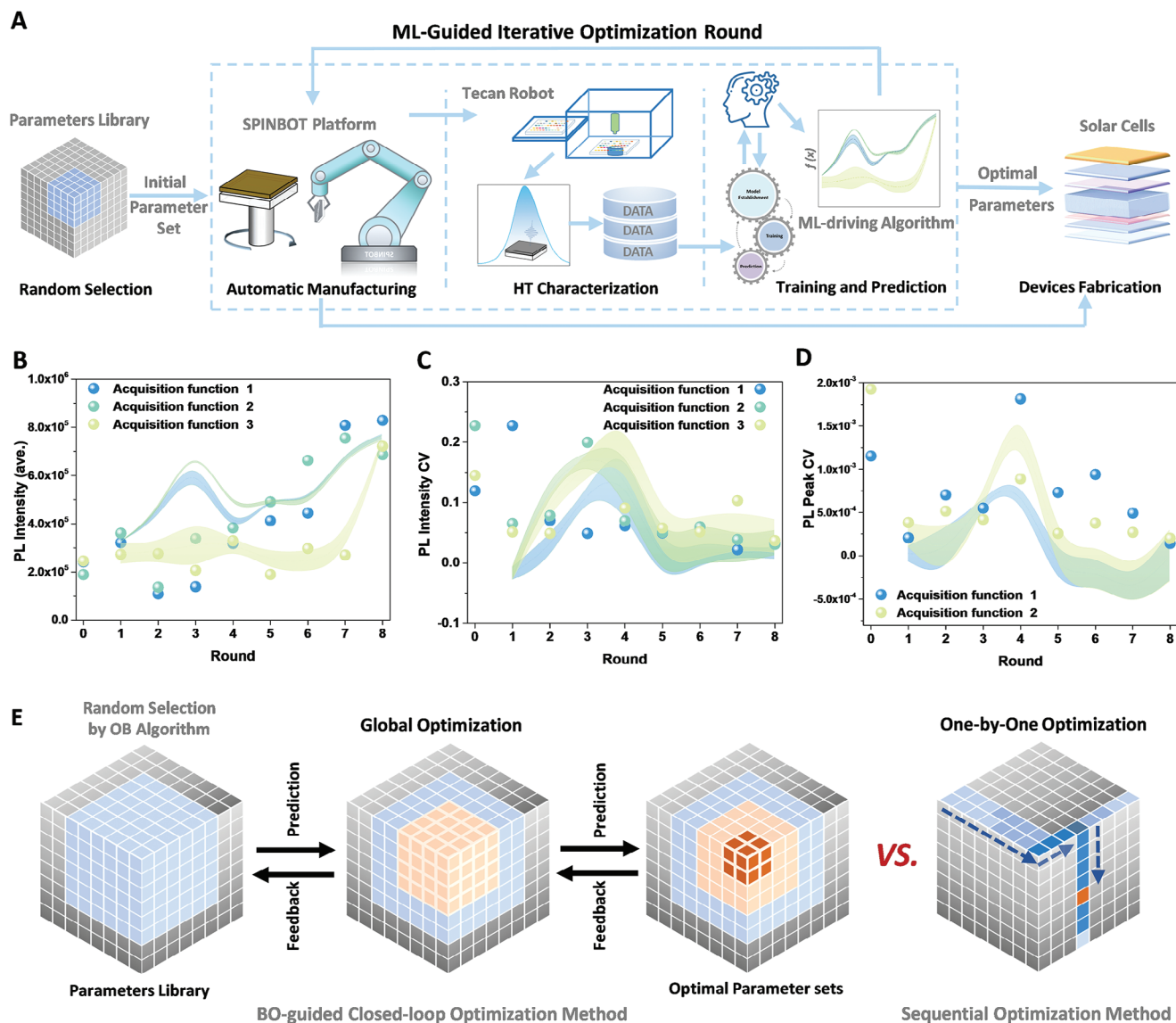


**Figure 3.** ML-guided closed-loop optimization for the film homogeneity and quality. A) Schematic of the BO-guided experimentation workflow. The workflow involves iterative optimization operations aimed at achieving high-quality and reproducible perovskite samples. B–D) Evolution of experimental PL peak CV, PL intensity, and PL intensity CV values, along with the corresponding prediction values and error ranges for Rounds 1–8. The color bands represent the predicted values with error ranges based on the most recent obtained values, as estimated by the BO algorithm. The solid balls of varying colors indicate the resulting experimental values. E) Schematic illustrating the BO-guided iterative optimization method and step-by-step method designed to achieve optimal parameters.

PCE of all champion devices in each group exceeds 19%, underpinning of high quality of the process implemented by the SPINBOT platform in ambient air. The grouped performance distribution of the devices is consistent with the analytical reproducibility of the results for the films produced in step 5–2. As shown in Figure 4B, the device with the optimum perovskite layer fabricated via the SPINBOT achieved PCE of 21.0%,  $V_{oc}$  of 1.1 V,  $J_{sc}$  of 23.7 mA cm<sup>-2</sup>, and FF of 80%, while the whole handcrafted (reference) PSCs exhibited PCE of 19.4%,  $V_{oc}$  of 1.07 V,  $J_{sc}$  of 23.5 mA cm<sup>-2</sup>, and FF of 77% (Figure S17, Supporting Information). By integrating the SPINBOT with the BO-based iterative optimization technique, we achieved outstanding device perfor-

mance with the optimal thin film, resulting in a champion PCE of 21.6%. The optimized devices exhibited exceptional performance metrics, including a  $V_{oc}$  of 1.13 V,  $J_{sc}$  of 24.5 mA cm<sup>-2</sup>, and FF of 78% (Figure 4C; Table S3, Supporting Information). These outcomes surpassed those obtained by the step-by-step optimization method, highlighting the efficacy of the BO-guided approach in maximizing film quality and device performance. Benefiting from the exceptional capabilities for process control of the automated platform, the devices fabricated on different days with the SPINBOT-optimized procedure show superior performance and reproducibility (Figure 4D; Figures S18 and S19, Supporting Information).

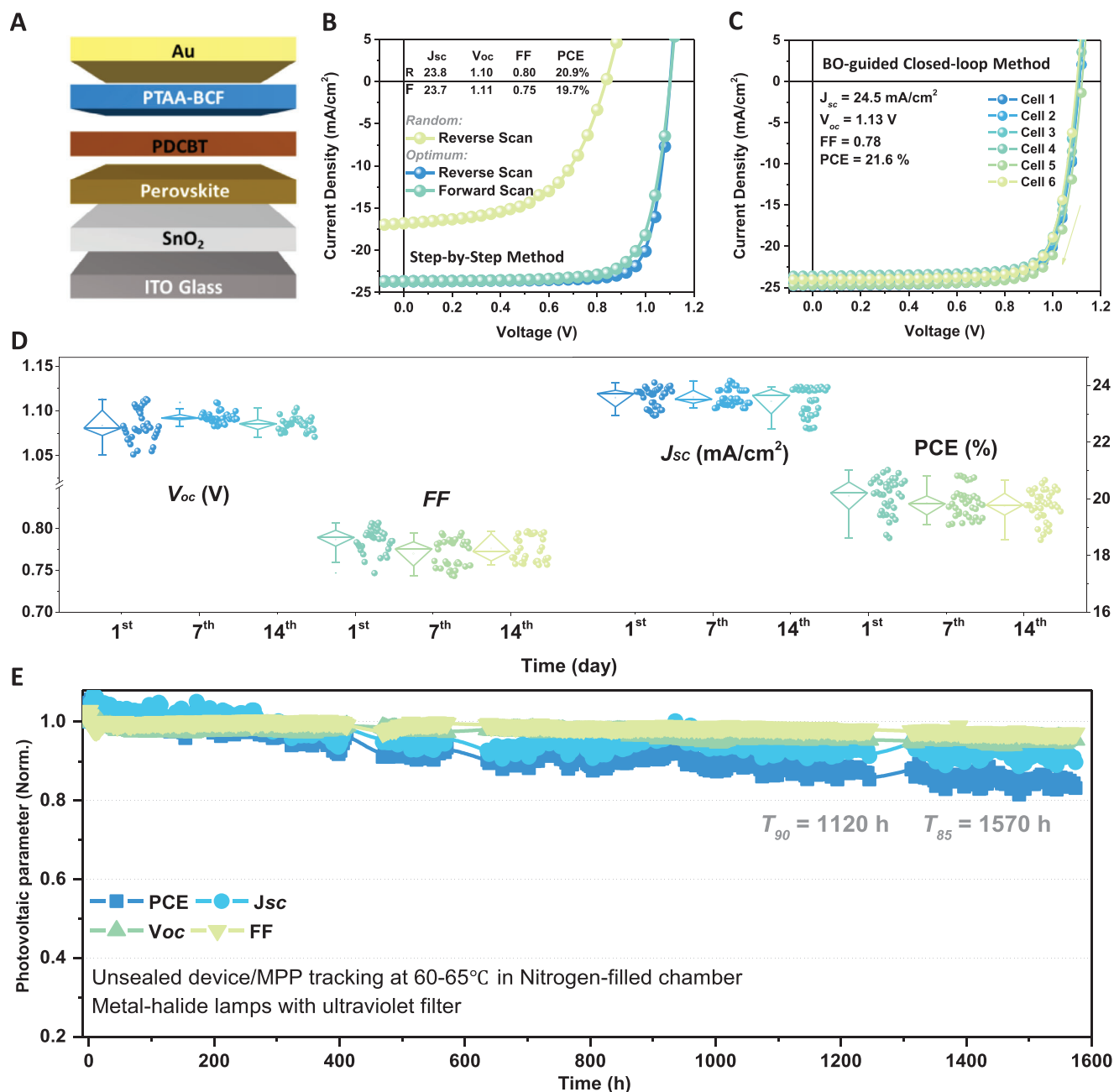


**Figure 4.** Device characterizations of PSCs with active layer produced via the SPINBOT in ambient air. A) Schematic of the metal halide PSCs structure. B)  $J$ - $V$  curves of the champion devices fabricated with the “optimal parameters” transferred from manual operation and the optimized parameters through the step-by-step method, respectively. (Insert text shows the detailed performance of the champion device. C)  $J$ - $V$  curves for the devices fabricated under the optimized parameters through the BO-guided closed-loop optimization technique. D) Grouped performance statistics for 36 solar cells fabricated under the optimum conditions at different times (the 1st, 7th, and 14th days, respectively). E) The best long-term stability of the unsealed device with optimal fabrication procedure tested at 60–65 °C in an  $N_2$ -filled chamber under metal-halide lamps (83  $mW\ cm^{-2}$ ) in reverse directions.

Another strong criterion of the quality of the layers and the corresponding defects is the operation lifetime at elevated temperatures. We decided to evaluate the long-term operational stability of unsealed devices with the perovskite layer fabricated via the SPINBOT. Here, we employed ISOS-L-3 (65 °C with MPP tracking, under light) protocols.<sup>[25,51]</sup> As shown in Figure 4E, after continuous aging at 60–65 °C in an  $N_2$ -filled chamber under metal-

halide lamps (83  $mW\ cm^{-2}$ ), the unencapsulated devices retained 90%  $\pm$  3% and 85%  $\pm$  3% of their initial efficiency after 1100 and 1570 h, respectively in both forward (Figure S20, Supporting Information) and reverse voltage scans. The results indicate that the optimization of the complete solar cell process using photoluminescence (PL) measurements is highly effective, signifying a noteworthy advancement in the realm of photovoltaics. We assert

that this methodology, coupled with the reliable automatic platform employed in our study, holds substantial value in providing guidance to both academia and industry. By offering insights on acceleration, our research has the potential to contribute significantly to advancements in the field.

### 3. Conclusion

We present the design and utilization of an automated platform, the SPINBOT, for the engineering of solution-processed functional thin films. The unique capabilities of this ML-guided platform were demonstrated by optimizing the manufacturing process of perovskite thin films within a complex multi-dimensional parameter space, utilizing fast PL proxy parameters for evaluation. By integrating the SPINBOT with a BO-based iterative optimization technique, we arrived at a film that, when processed into a device in an ambient atmosphere, immediately yielded a champion efficiency of 21.6% in an unsealed device with satisfactory photo-thermal stability and performance reproducibility. Our next goal is to expand the capabilities of the SPINBOT to enable autonomous optimization experiments for multilayer systems, leveraging artificial intelligence (AI) for experiment design. Through this advancement, we anticipate facilitating the material and process development for environmentally processed and performance-optimized electronics such as perovskite devices. We believe the robotic scientist paradigm offered by the SPINBOT opens up new possibilities in materials science, providing researchers with a powerful tool to accelerate the discovery and optimization of functional thin films. This advancement has the potential to revolutionize various fields, including electronics, energy, and optoelectronics, by enabling rapid prototyping, efficient process development, and the exploration of novel materials and device architectures.

### Supporting Information

Supporting Information is available from the Wiley Online Library or from the author.

### Acknowledgements

J.Z., J.A.H., and C.J.B. gratefully acknowledge the grants AutoPeroSol (ZT-I-PF-3-020) and AI-InSu-Pero (ZT-I-PF-5-106) by the Helmholtz Foundation. J.Z. and K.Z., gratefully acknowledge financial support from the China Scholarship Council (CSC). J.C.W. and J.L. are grateful for financial support from the Sino-German Postdoc Scholarship Program (CSC-DAAD). J.L. gratefully acknowledges financial support from the National Natural Science Foundation of China (Grant No. 62104031) and the Technical Field Funds of 173 Project (Grant No. 24JJ210663A). J.A.H., Y.Z., and C.J.B. gratefully acknowledge the grants “ELF-PV-Design and development of solution-processed functional materials for the next generations of PV technologies” (No. 44–6521a/20/4) by the Bavarian State Government. C.M.S.-F. acknowledges support by the Molecular Foundry supported by the Office of Science, Office of Basic Energy Sciences, of the U.S. Department of Energy under Contract No. DE-AC02-05CH11231. C.J.B. gratefully acknowledges financial support through the “Aufbruch Bayern” initiative of the state of Bavaria (EnCN and “Solar Factory of the Future”), the Bavarian Initiative “Solar Technologies go Hybrid” (SolTech), and the German Research Foundation (DFG) SFB 953—No. 182849149.

Open access funding enabled and organized by Projekt DEAL.

### Conflict of Interest

The authors declare no conflict of interest.

### Author Contributions

The study was conceptualized by J.Z., Y.Z., and C.J.B., J.Z., and Y.Z. designed the optimization experiments. J.Z., B.L., and S.A. performed the thin film fabrication. J.Z. carried out the HT characterization experiments. J.Z., Z.L., and Y.Z. implemented the BO-guided closed-loop optimization. J.Z., B.L., H.S., and Z.W. prepared the solutions. J.Z. fabricated the devices. J.Z., J.L., and T.H. performed the device's stability test. J.Z., Y.Z., Z.L., and J.C.W. analyzed the data. T.S., J.W., C.G.B., S.A., and T.O. established and smoothed the SPINBOT platform. J.A.H., Y.Z., and C.J.B. supervised the project. J.Z. made the figures and wrote the manuscript, J.A.H., C.M.S.-F., I.M.P., Y.Z., and C.J.B. contributed mainly to the revision of the manuscript. J.C.W., S.A., T.O., F.S., and K.Z. contributed to the editing of this manuscript. All authors contributed to the discussion of experimental results and the manuscript.

### Data Availability Statement

The data that support the findings of this study are available in the supplementary material of this article or from the corresponding authors upon reasonable request.

### Keywords

closed-loop optimization, efficient and stable devices, machine learning, manufacturing optimization, perovskite thin films, PL characterization, robotic platform

Received: August 8, 2023

Revised: October 4, 2023

Published online: November 1, 2023

- [1] R. Sun, T. Wang, X. Yang, Y. Wu, Y. Wang, Q. Wu, M. Zhang, C. J. Brabec, Y. Li, J. Min, *Nat. Energy* **2022**, *7*, 1087
- [2] Y. He, N. Li, T. Heumüller, J. Wortmann, B. Hanisch, A. Aubele, S. Lucas, G. Feng, X. Jiang, W. Li, P. Bäuerle, C. J. Brabec, *Joule* **2022**, *6*, 1160.
- [3] C. Liu, X. Du, S. Gao, A. Classen, A. Osvet, Y. He, K. Mayrhofer, N. Li, C. J. Brabec, *Adv. Energy Mater.* **2020**, *10*, 1903800.
- [4] Y. Ren, D. Zhang, J. Suo, Y. Cao, F. T. Eickemeyer, N. Vlachopoulos, S. M. Zakeeruddin, A. Hagfeldt, M. Grätzel, *Nature* **2023**, *613*, 60.
- [5] A. Hagfeldt, G. Boschloo, L. Sun, L. Kloo, H. Pettersson, *Chem. Rev.* **2010**, *110*, 6595.
- [6] N. Rolston, W. J. Scheideler, A. C. Flick, J. P. Chen, H. Elmaraghi, A. Sleugh, O. Zhao, M. Woodhouse, R. H. Dauskardt, *Joule* **2020**, *4*, 2675.
- [7] W. Meng, K. Zhang, A. Osvet, J. Zhang, W. Gruber, K. Forberich, B. Meyer, W. Heiss, T. Unruh, N. Li, C. J. Brabec, *Joule* **2022**, *6*, 458.
- [8] Z. A. Vanorman, L. Nienhaus, *InfoMat* **2021**, *3*, 962.
- [9] Z. Saki, M. M. Byranvand, N. Taghavinia, M. Kedia, M. Saliba, *Energy Environ. Sci.* **2021**, *14*, 5690.
- [10] A. Aspuru-Guzik, K. Persson, Materials Acceleration Platform: Accelerating Advanced Energy Materials Discovery by Integrating High-Throughput Methods and Artificial Intelligence. Mission Innovation, <https://dash.harvard.edu/handle/1/35164974>, (accessed: January 2018).

- [11] B. Cao, L. A. Adutwum, A. O. Olynyk, E. J. Lubber, B. C. Olsen, A. Mar, J. M. Buriak, *ACS Nano* **2018**, *12*, 7434.
- [12] H.-C. Choi, H. Yun, J.-S. Yoon, R.-H. Baek, *IEEE Access* **2020**, *8*, 159351.
- [13] K. P. Goetz, Y. Vaynzof, *ACS Energy Lett.* **2022**, *7*, 1750.
- [14] M. Awais, D. Thrithamarassery Gangadharan, F. Tan, M. I. Saidaminov, *Chem. Mater.* **2022**, *34*, 8112.
- [15] R. D. King, K. E. Whelan, F. M. Jones, P. G. K. Reiser, C. H. Bryant, S. H. Muggleton, D. B. Kell, S. G. Oliver, *Nature* **2004**, *427*, 247.
- [16] B. Burger, P. M. Maffettone, V. V. Gusev, C. M. Aitchison, Y. Bai, X. Wang, X. Li, B. M. Alston, B. Li, R. Clowes, N. Rankin, B. Harris, R. S. Sprick, A. I. Cooper, *Nature* **2020**, *583*, 237.
- [17] A.-C. Bédard, A. Adamo, K. C. Aroh, M. G. Russell, A. A. Bedermann, J. Torosian, B. Yue, K. F. Jensen, T. F. Jamison, *Science* **2018**, *361*, 1220.
- [18] D. P. Tabor, L. M. Roch, S. K. Saikin, C. Kreisbeck, D. Sheberla, J. H. Montoya, S. Dwaraknath, M. Aykol, C. Ortiz, H. Tribukait, C. Amador-Bedolla, C. J. Brabec, B. Maruyama, K. A. Persson, A. Aspuru-Guzik, *Nat. Rev. Mater.* **2018**, *3*, 5.
- [19] B. P. MacLeod, F. G. L. Parlane, A. K. Brown, J. E. Hein, C. P. Berlinguette, *Nat. Mater.* **2022**, *21*, 722.
- [20] C. W. Coley, D. A. Thomas, J. A. M. Lummiss, J. N. Jaworski, C. P. Breen, V. Schultz, T. Hart, J. S. Fishman, L. Rogers, H. Gao, R. W. Hicklin, P. P. Plehiers, J. Byington, J. S. Piotti, W. H. Green, A. J. Hart, T. F. Jamison, K. F. Jensen, *Science* **2019**, *365*, eaax1566.
- [21] J. Yang, B. J. Lawrie, S. V. Kalinin, M. Ahmadi, *Adv. Energy Mater.* **2023**, <https://doi.org/10.1002/aenm.202302337>.
- [22] B. P. Macleod, F. G. L. Parlane, T. D. Morrissey, F. Häse, L. M. Roch, K. E. Dettelbach, R. Moreira, L. P. E. Yunker, M. B. Rooney, J. R. Deeth, V. Lai, G. J. Ng, H. Situ, R. H. Zhang, M. S. Elliott, T. H. Haley, D. J. Dvorak, A. Aspuru-Guzik, J. E. Hein, C. P. Berlinguette, *Sci. Adv.* **2020**, *6*, eaaz8867.
- [23] B. P. Macleod, F. G. L. Parlane, C. C. Rupnow, K. E. Dettelbach, M. S. Elliott, T. D. Morrissey, T. H. Haley, O. Proskurin, M. B. Rooney, N. Taherimaksousi, D. J. Dvorak, H. N. Chiu, C. E. B. Waizenegger, K. Ocean, M. Mokhtari, C. P. Berlinguette, *Nat. Commun.* **2022**, *13*, 995.
- [24] H. Zhao, W. Chen, H. Huang, Z. Sun, Z. Chen, L. Wu, B. Zhang, F. Lai, Z. Wang, M. L. Adam, C. H. Pang, P. K. Chu, Y. Lu, T. Wu, J. Jiang, Z. Yin, X.-F. Yu, *Nat. Synth.* **2023**, *2*, 505.
- [25] Y. Zhao, T. Heumueller, J. Zhang, J. Luo, O. Kasian, S. Langner, C. Kupfer, B. Liu, Y. Zhong, J. Elia, A. Osvet, J. Wu, C. Liu, Z. Wan, C. Jia, N. Li, J. Hauch, C. J. Brabec, *Nat. Energy* **2022**, *7*, 144.
- [26] Y. Zhao, J. Zhang, Z. Xu, S. Sun, S. Langner, N. T. P. Hartono, T. Heumueller, Y. Hou, J. Elia, N. Li, G. J. Matt, X. Du, W. Meng, A. Osvet, K. Zhang, T. Stubhan, Y. Feng, J. Hauch, E. H. Sargent, T. Buonassisi, C. J. Brabec, *Nat. Commun.* **2021**, *12*, 2191.
- [27] C. Liu, L. Lüer, V. M. L. Corre, K. Forberich, P. Weitz, T. Heumueller, X. Du, J. Wortmann, J. Zhang, J. Wagner, L. Ying, J. Hauch, N. Li, C. J. Brabec, *Adv. Mater.* **2023**, <https://doi.org/10.1002/adma.202300259>.
- [28] X. Du, L. Lüer, T. Heumueller, J. Wagner, C. Berger, T. Osterrieder, J. Wortmann, S. Langner, U. Vongsaysy, M. Bertrand, N. Li, T. Stubhan, J. Hauch, C. J. Brabec, *Joule* **2021**, *5*, 495.
- [29] S. Sun, N. T. P. Hartono, Z. D. Ren, F. Oviedo, A. M. Buscemi, M. Layurova, D. X. Chen, T. Ogunfunmi, J. Thapa, S. Ramasamy, C. Settens, B. L. Decost, A. G. Kusne, Z. Liu, S. I. P. Tian, I. M. Peters, J.-P. Correa-Baena, T. Buonassisi, *Joule* **2019**, *3*, 1437.
- [30] Z. Liu, N. Rolston, A. C. Flick, T. W. Colburn, Z. Ren, R. H. Dauskardt, T. Buonassisi, *Joule* **2022**, *6*, 834.
- [31] N. Meftahi, M. A. Surmiak, S. O. Furer, K. J. Rietwyk, J. Lu, S. R. Raga, C. Evans, M. Michalska, H. Deng, D. P. McMeekin, T. Alan, D. Vak, A. S. R. Chesman, A. J. Christofferson, D. A. Winkler, U. Bach, S. P. Russo, *Adv. Energy Mater.* **2023**, *13*, 2370154.
- [32] P. M. Attia, A. Grover, N. Jin, K. A. Severson, T. M. Markov, Y.-H. Liao, M. H. Chen, B. Cheong, N. Perkins, Z. Yang, P. K. Herring, M. Aykol, S. J. Harris, R. D. Braatz, S. Ermon, W. C. Chueh, *Nature* **2020**, *578*, 397.
- [33] A. E. Gongora, B. Xu, W. Perry, C. Okoye, P. Riley, K. G. Reyes, E. F. Morgan, K. A. Brown, *Sci. Adv.* **2020**, *6*, eaaz1708.
- [34] R. Ramprasad, R. Batra, G. Paliana, A. Mannodi-Kanakkithodi, C. Kim, *NPJ Comput. Mater.* **2017**, *3*, 54.
- [35] J. Snoek, H. Larochele, R. P. Adams, *Adv. Neural Inf. Process.* **2012**, *25*, 2951.
- [36] L. Zhi, N. Mansoor Ani, A. Liana, S. Alyssa, P. Peter Cruz, P. M. Ian, Z. Matthias, S. Joshua, N. J. Alexander, C. Emory, *Chem. Mater.* **2020**, *32*, 5650.
- [37] J.-P. Correa-Baena, K. Hippalgaonkar, J. Van Duren, S. Jaffer, V. R. Chandrasekhar, V. Stevanovic, C. Wadia, S. Guha, T. Buonassisi, *Joule* **2018**, *2*, 1410.
- [38] J. Wagner, C. G. Berger, X. Du, T. Stubhan, J. A. Hauch, C. J. Brabec, *J. Mater. Sci.* **2021**, *56*, 16422.
- [39] J. Zhang, S. Langner, J. Wu, C. Kupfer, L. Lüer, W. Meng, B. Zhao, C. Liu, M. Daum, A. Osvet, N. Li, M. Halik, T. Stubhan, Y. Zhao, J. A. Hauch, C. J. Brabec, *ACS Energy Lett.* **2022**, *7*, 70.
- [40] S. Langner, F. Häse, J. D. Perea, T. Stubhan, J. Hauch, L. M. Roch, T. Heumueller, A. Aspuru-Guzik, C. J. Brabec, *Adv. Mater.* **2020**, *32*, 1907801.
- [41] J. Zhang, J. Wu, S. Langner, B. Zhao, Z. Xie, J. A. Hauch, H. A. Affy, A. Barabash, J. Luo, M. Sytnyk, W. Meng, K. Zhang, C. Liu, A. Osvet, N. Li, M. Halik, W. Heiss, Y. Zhao, C. J. Brabec, *Adv. Funct. Mater.* **2022**, *32*, 2207101.
- [42] Z. Xu, Y. Zhao, J. Zhang, K. Chen, C. J. Brabec, Y. Feng, *Phys. Rev. Mater.* **2020**, *4*, 095401.
- [43] J. Wu, J. Zhang, M. Hu, P. Reiser, L. Torresi, P. Friederich, L. Lahn, O. Kasian, D. M. Guldi, M. E. Pérez-Ojeda, A. Barabash, J. S. Rocha-Ortiz, Y. Zhao, Z. Xie, J. Luo, Y. Wang, S. I. Seok, J. A. Hauch, C. J. Brabec, *J. Am. Chem. Soc.* **2023**, *145*, 16517.
- [44] J. Zhang, J. Wu, Y. Zhao, Y. Zou, A. Barabash, Z. Wu, K. Zhang, C. Deng, J. Elia, C. Li, J. S. Rocha-Ortiz, C. Liu, A. Saboor, I. M. Peters, J. A. Hauch, C. J. Brabec, *ACS Energy Lett.* **2023**, *8*, 3595.
- [45] D. W. De Quillettes, S. M. Vorpahl, S. D. Stranks, H. Nagaoka, G. E. Eperon, M. E. Ziffer, H. J. Snaith, D. S. Ginger, *Science* **2015**, *348*, 683.
- [46] W. Zhang, S. Pathak, N. Sakai, T. Stergiopoulos, P. K. Nayak, N. K. Noel, A. A. Haghghirad, V. M. Burlakov, D. W. DeQuillettes, A. Sadhanala, W. Li, L. Wang, D. S. Ginger, R. H. Friend, H. J. Snaith, *Nat. Commun.* **2015**, *6*, 10030.
- [47] C. Momblona, L. Gil-Escrig, E. Bandiello, E. M. Hutter, M. Sessolo, K. Lederer, J. Blochwitz-Nimoth, H. J. Bolink, *Energy Environ. Sci.* **2016**, *9*, 3456.
- [48] X. Li, D. Bi, C. Yi, J.-D. Décoppet, J. Luo, S. M. Zakeeruddin, A. Hagfeldt, M. Grätzel, *Science* **2016**, *353*, 58.
- [49] A. G. Bedeian, K. W. Mossholder, *Organ. Res. Methods* **2000**, *3*, 285.
- [50] J. Zhang, W. Liang, W. Yu, S. Yu, Y. Wu, X. Guo, S. F. Liu, C. Li, *Small* **2018**, *14*, 1800181.
- [51] M. V. Khenkin, E. A. Katz, A. Abate, G. Bardizza, J. J. Berry, C. Brabec, F. Brunetti, V. Bulovic, Q. Burlingame, A. Di Carlo, R. Cheacharoen, Y.-B. Cheng, A. Colmann, S. Cros, K. Domanski, M. Duszka, C. J. Fell, S. R. Forrest, Y. Galagan, D. Di Girolamo, M. Grätzel, A. Hagfeldt, E. Von Hauff, H. Hoppe, J. Kettle, H. Köbler, M. S. Leite, S. Liu, Y.-L. Loo, J. M. Luther, et al., *Nat. Energy* **2020**, *5*, 35.